# High-energy Emission from Pulsar Magnetospheres

HIROTANI, Kouichi

ASIAA/TIARA, Taiwan

The Sixth Workshop on Black Hole Magnetospheres
March 7, 2013

Crab nebula: Composite image of X-ray [blue] and optical [red]

## §1 γ-ray Pulsar Observations

After 2008, LAT aboard Fermi has detected more than 100 pulsars above 100 MeV.


Fermi/LAT point sources (>100 MeV)

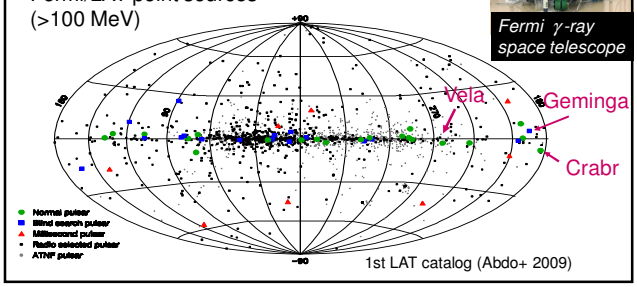


1st LAT catalog (Abdo+ 2009)

## §1 γ-ray Pulsar Observations

Recent IACTs found pulsed emission in 25-400 GeV from the Crab pulsar.

VERITAS ( > 120 GeV)
Aliu+ (2011, Science 334, 69)

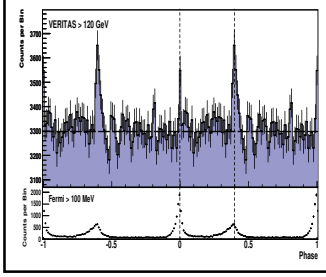


MAGIC (25–416 GeV)
Aleksić+ (2011a,b)

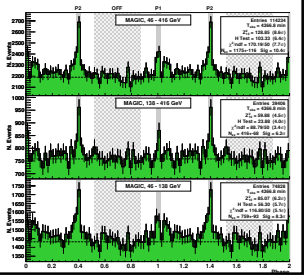


## Broad-band spectra (pulsed)

- High-energy (>100MeV) photons are emitted mainly via **curvature** process by ultra-relativistic $e^{\pm}$'s.
- Above several GeV, curvature spectrum should show exp. cutoff.

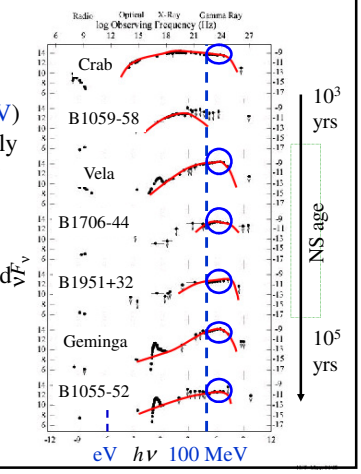

## *Broad-band spectra (pulsed)*

- High-energy (>100MeV) photons are emitted mainly via **curvature** process by ultra-relativistic $e^{\pm}$'s.
- Above several GeV, curvature spectrum should show exp. cutoff.
- However, above 20 GeV, **ICS by secondary/tertiary pairs** contributes.

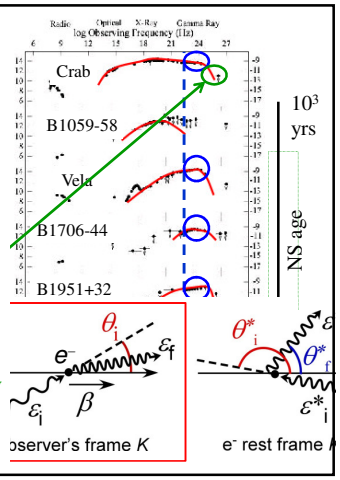


## *Broad-band spectra (pulsed)*

- High-energy (>100MeV) photons are emitted mainly via **curvature** process by ultra-relativistic (~10TeV) $e^{\pm}$'s accelerated in pulsar magnetosphere.
- Some of the **primary** γ-rays are absorbed in the NS magnetosphere and reprocessed in lower energies via **synchrotron** process.

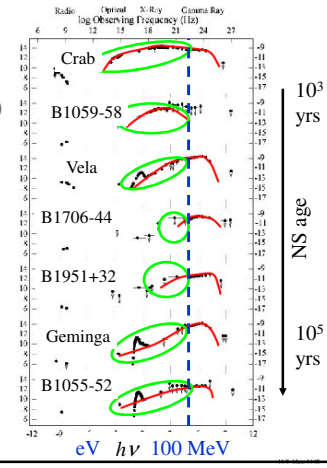


## §2 *Rotating NS Magnetosphere*

The observed high-energy emissions are realized when the rotational energy of the NS is electro-dynamically extracted and partly dissipated in the magnetosphere.

(e.g., unipolar inductor)

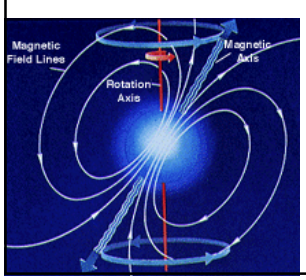


Magnetic and rotation axes are generally misaligned.

**Pulsars**:
rapidly rotating, highly magnetized NS

## §2 *Rotating NS Magnetosphere*

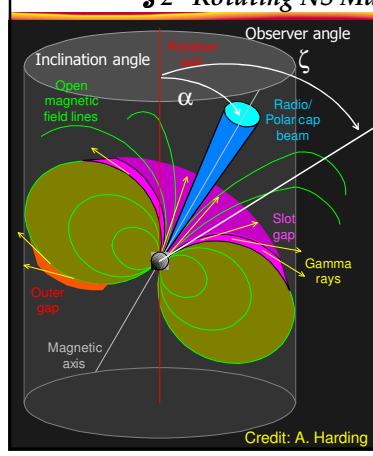


Possible sites of particle acceleration

- Ideal MHD condition holds in most of magnetosphere, $E \cdot B = 0$.
- In some limited regions, deficient charge supply leads to $E \cdot B \neq 0$.
- In charge deficit region, $E_{\parallel}$ is solved from the Poisson eq., $\nabla \cdot E_{\parallel} = 4\pi(\rho - \rho_{GJ})$.

## §2 Rotating NS Magnetosphere

Early 80's, the polar-cap (PC) model was proposed.
(Daugherty & Harding ApJ 252, 337, 1982)

A single PC beam can produce a variety of pulse profiles.

However, the emission solid angle ($\Delta\Omega$ «1 ster) was too small to reproduce the wide-separated double peaks.

A great deal of effort has been made; however, one has to invoke a very small inclination, $\alpha$, and viewing angles, $\zeta$, to reproduce the widely separated pulse peaks.

In addition, localization of gap altitudes (« $r_*$) prohibits enough $L_\gamma$ (<0.3$L_{spin}$) as observed. ($L_{radio}$~$10^{-5}L_{spin}$ is OK.)

Thus, a high-altitude emission drew attention.

## §3 Higher-altitude Pulsar Emission Models

Big breakthrough: Muslimov & Tsygan (1992, MN 255, 61) found that a polar gap can extend into the higher altitudes by virtue of the frame-dragging effect.

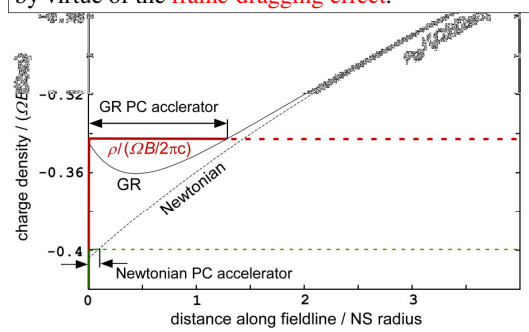


## §3 Higher-altitude Pulsar Emission Models

Extending the original idea of Arons (1983, ApJ 266, 215), Muslimov & Harding (2003, ApJ 588, 430) proposed the lower-altitude slot-gap (SG) model.

Slot gap = a pair-free space formed between the last-open field lines and the pair-formation front (PFF).

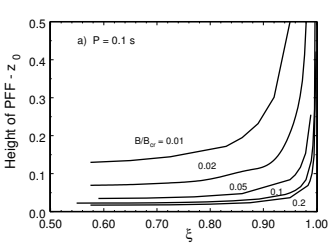


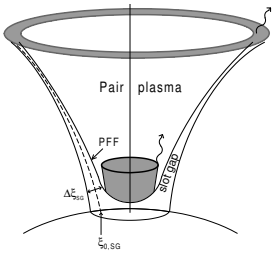


## §3 Higher-altitude Pulsar Emission Models

However, a lower-altitude SG is still limited within a few $r_*$.
Thus, the same difficulty ($\Delta\Omega$ «1 ster) still remains.

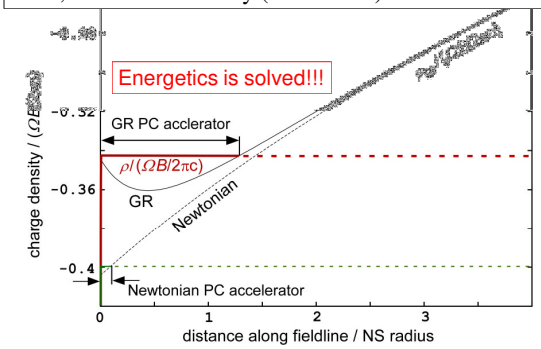

## §3 Higher-altitude Pulsar Emission Models

To contrive a higher-altitude emission model, Muslimov & Harding (2004a, ApJ 606, 1143; 2004b, ApJ 617, 471) and Dyks, Harding & Rudak (2004, ApJ 606, 1125) extended the lower-altitude slot-gap solution into higher altitudes (in fact, by hand).

They explained, e.g., the widely separated double peaks.

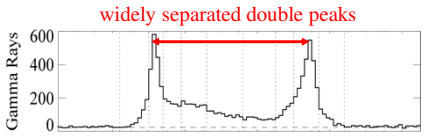


## §3 Higher-altitude Pulsar Emission Models

Assuming that the gap extends from the NS surface to the light cylinder with constant emissivity, Dyks & Rudak (2003, ApJ 598, 1201) demonstrated the formation of double peaks, which arise from the crossing of two caustics associated with different poles.

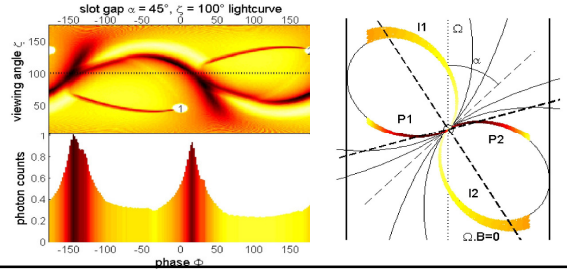


## §3 Higher-altitude Pulsar Emission Models

Assuming that the gap extends from the NS surface to the light cylinder with constant emissivity, Dyks & Rudak (2003, ApJ 598, 1201) demonstrated the formation of double peaks.

In this higher-altitude slot-gap model, most observers catch emission from both (N/S) poles.

trailing-side emission → main peaks
leading-side emission → inter-peak & off-pulse

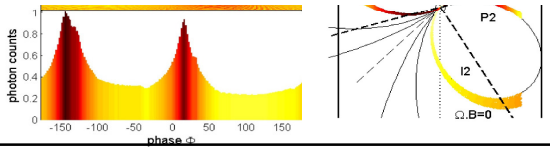


## §3 Higher-altitude Pulsar Emission Models

Dyks, Harding, Rudak (2004, ApJ 606, 1125) showed that Crab pulsar's optical polarization characteristics can be qualitatively reproduced by their SG model.

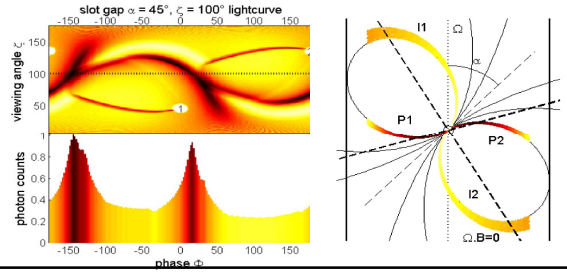

## §3 Higher-altitude Pulsar Emission Models

Dyks, Harding, Rudak (2004, ApJ 606, 1125) showed that Crab pulsar's optical polarization characteristics can be qualitatively reproduced by their SG model.

Harding+ (2008, ApJ ApJ 680, 1378) examined Crab's γ-ray emission and found that the pulse profiles and the phase-resolved spectrum are qualitatively reproduced.

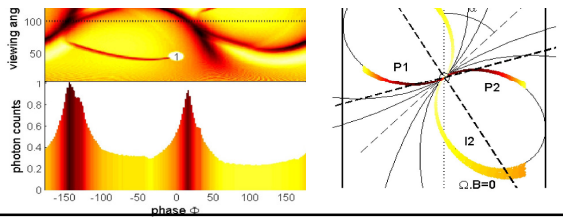


## §3 Higher-altitude Pulsar Emission Models

Dyks, Harding, Rudak (2004, ApJ 606, 1125) showed that Crab pulsar's optical polarization characteristics can be qualitatively reproduced by their SG model.

Harding+ (2008, ApJ ApJ 680, 1378) examined Crab's γ-ray emission and found that the pulse profiles and the phase-resolved spectrum are qualitatively reproduced.

However, unfortunately, the higher-altitude SG model contains two fatal electro-dynamical inconsistencies.

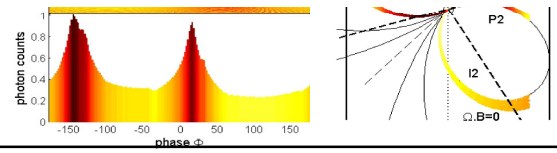


## §4 Difficulties in Higher-altitude SG Model

**Problem 1: insufficient luminosity** KH (2008) ApJ 688, L25

Adopting the same parameter as Harding+(2008), one obtains too small γ-ray flux from a higher-altitude SG.

Fig. Phase-averaged SG spectrum for four discrete viewing angles, 90°, 100°, 110°, and 120°.

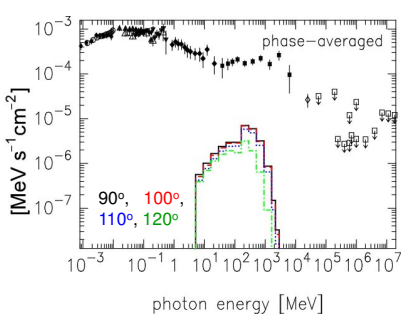


## §4 Difficulties in Higher-altitude SG Model

**Problem 1: insufficient luminosity** KH (2008) ApJ 688, L25

Adopting the same parameter as Harding+(2008), one obtains too small γ-ray flux from a higher-altitude SG.

Analytically predicted γ-ray flux of the Crab pulsar:

$$(\nu F_\nu)_{\rm peak} \approx 0.0450 f^3 \kappa \underbrace{\frac{\mu^2\Omega^4}{c^3}\frac{1}{d^2}}_{\propto \dot{E}/d^2\,:\ \text{spin-down flux}}, \qquad \kappa \sim 1.$$

$f$: fractional gap width ($f \ll 1$ denotes a thin gap)

The difference between OG and SG models appears through $f$, $\kappa$, and assumed $\mu$ (magnetic moment).

## §4 Difficulties in Higher-altitude SG Model

**Problem 1: insufficient luminosity** KH (2008) ApJ 688, L25

$$(\nu F_\nu)_{\rm peak} \approx 0.0450 f^3 \kappa \frac{\mu^2 \Omega^4}{c^3} \frac{1}{d^2}$$

Apply this general result to the Crab pulsar ($\Omega$=190 rad s$^{-1}$).

(I) For OG model ($f$~0.14, $\kappa$~0.3, $\mu$=4×10$^{30}$ G cm$^3$),

$(\nu F_\nu)_{\rm peak}$ ~ 4×10$^{-4}$ MeV s$^{-1}$ cm$^{-2}$ ~ EGRET flux.

(II) For SG model ($f$~0.04, $\kappa$~0.2), even with a large $\mu$,

$(\nu F_\nu)_{\rm peak}$ ~ 3×10$^{-5}$ ($\mu$/8 × 10$^{30}$)$^2$ MeV s$^{-1}$ cm$^{-2}$

< 0.1 EGRET flux.

## §4 Difficulties in Higher-altitude SG Model

**Problem 1: insufficient luminosity**

In short, both analytical and numerical results show that **a SG can produce a negligible γ-ray flux.**

(I) For OG model ($f$~0.14, $\kappa$~

$(\nu F_\nu)_{\rm peak}$ ~ 4×10$^{-4}$ MeV

(II) For SG model ($f$~0.04, $\kappa$~

$(\nu F_\nu)_{\rm peak}$ ~ 3×10$^{-5}$ ($\mu$/8 ×

< 0.1 EGRET fl

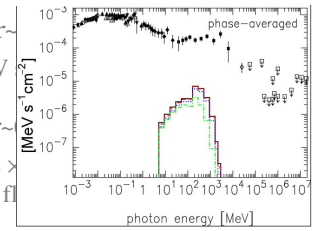


OG model remains as the only possible γ-ray pulsar model.

KH (2008) ApJ 688, L25

## §5 Difficulties in Higher-altitude SG Model

**Problem 2: unphysical assumption of GJ charge density (per *B* flux tube)**

Without pair creation, electron density per B will be constant along the field line. However, it results in a reversal of $E_\parallel$ due to the sign change of $\rho - \rho_{\rm GJ}$.

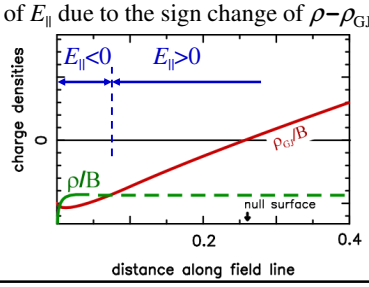


## §5 Difficulties in Higher-altitude SG Model

**Problem 2: unphysical assumption of $\rho_{\rm GJ}$/B**

To prevent a sign reversal of $E_\parallel$, they assumed that $\rho_{\rm GJ}$/B tends to a constant in the higher altitudes

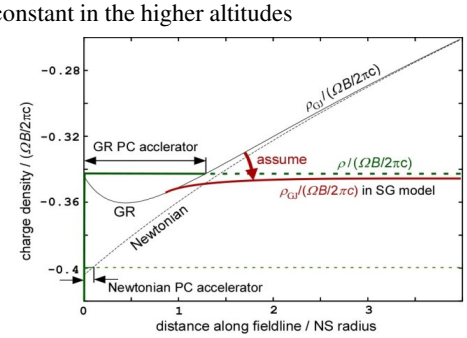

## §5 Difficulties in Higher-altitude SG Model

**Problem 2: unphysical assumption of $\rho_{GJ}$/B**

To prevent a sign reversal of $E_{\|}$, they assumed that $\rho_{GJ}$/B tends to a constant in the higher altitudes.

However, Maxwell eq. uniquely gives

$$\rho_{GJ} = \frac{c^2}{4\pi\sqrt{-g}}\partial_\mu\left(\frac{\sqrt{-g}}{\rho_w^2}g^{\mu\nu}g_{\varphi\varphi}(\Omega-\omega)F_{\varphi\nu}\right).$$

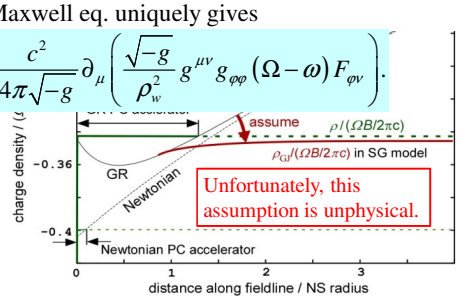


## §5 Difficulties in Higher-altitude SG Model

**Problem 2: unphysical assumption of $\rho_{GJ}$/B**

Since the pair-starved PC (PSPC) model adopts the same $\rho_{GJ}$ distribution, this difficulty applies not only to the higher-altitude SG model, but also to the PSPC model (Venter+ 2009, ApJ 707, 800).

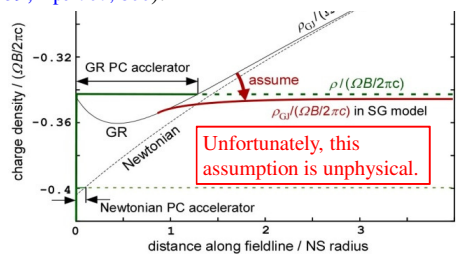


## §5 Difficulties in Higher-altitude SG Model

**Problem 2: unphysical assumption of $\rho_{GJ}$/B**

Since the pair-starved PC (PSPC) model adopts the same $\rho_{GJ}$ distribution, this difficulty applies not only to the higher-altitude SG model, but also to the PSPC model (Venter+ 2009, ApJ 707, 800).

In short, higher-latitude SG model & PSPC model contain serious electro-dynamical problem that contradicts with Maxwell eq.

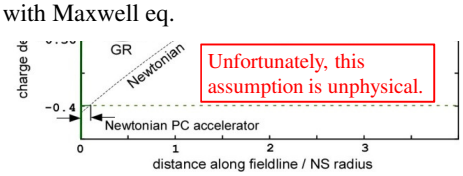


## §6 Classic Outer-gap (OG) Models

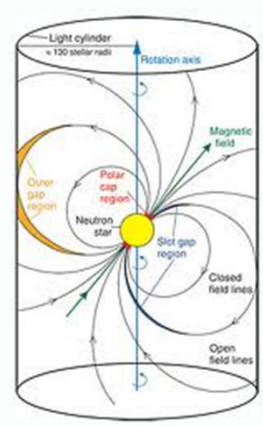


As an alternative possibility of high-altitude emission model, the outer gap model was proposed.

Cheng, Ho, Ruderman (1986, ApJ 300, 500)

So far, there have been found no serious electrodynamical problems in the OG model (unlike SG or PSPC model).

Thus, let us concentrate on the OG model in what follows.

## §6 Classic OG Models

Mid 80's, the outer-gap (OG) model was proposed.
(Cheng, Ho, Ruderman ApJ 300, 500, 1986)

Emission altitude > 100 $r_{NS}$ ⟶ hollow cone emission
($\Delta\Omega > 1$ ster)

Mid 90s', OG model was further developed by including special relativistic effects. (Romani ApJ 470, 469)

⟶ Explains wide-separated double peaks.

Outer-gap model became promising.

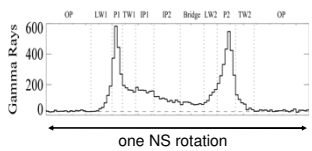


## §7 Modern Outer-Gap Model

Indeed, the sub-TeV components from the Crab pulsar shows that pulsed γ-rays are emitted from the **outer** magnetosphere (~~γB→ee~~).

We thus consider the outer-gap model (Cheng+ 86, ApJ 300,500) in this talk.

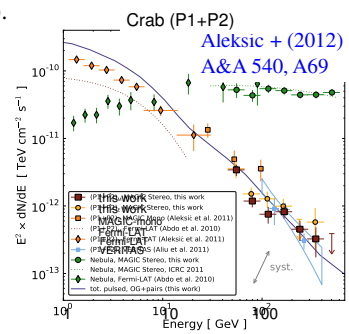


## §7 Modern Outer-Gap Model

Various attempts have been made on recent OG model:

3-D geometrical model
→ phase-resolved spectra (Cheng + '00; Tang + '08)
→ atlas of light curves for PC, OG, SG models (Watters + '08)

2-D self-consistent solution (Takata + '06; KH '06)

3-D self-consistent solution
→ phase-resolved spectra, absolute luminosity if we give only $P$, $dP/dt$, $\alpha$, $kT$ ($+\zeta$) (this talk)

In this talk, I'll present the most recent results obtained in my 3-D version of self-consistent OG calculations.

## §7 Modern Outer-Gap Model

**3-D self-consistent OG model**

Death line of normal and millisecond PSRs on ($P$,$\dot{P}$) plane
(Wang & KH 2011, ApJ 736, 127)

Spectral hardening of trailing light-curve peak
(KH 2011, ApJ 733, L49)

Crab pulsars HE-VHE pulsed inverse-Compton emission
(Alkesic + 2011, ApJ 742, 43)
(Alkesic + 2012, AA 540, A69)

Evolution of γ-ray luminosity of rotation-powered PSRs
(KH 2013, ApJ in press)

## §7 Modern OG Model: Lγ vs. $L_{spin}$

Today, using the OG mode, we derive the observed relationship, $L_\gamma \propto L_{spin}^{0.5}$, both analytically and numerically.

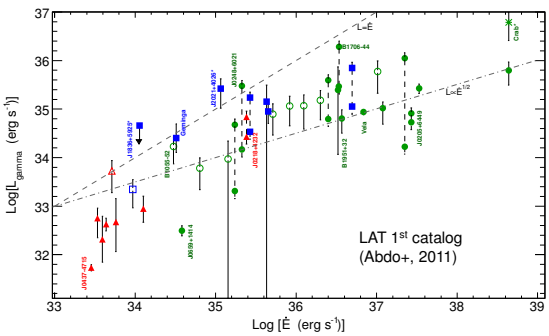


## §7 Modern OG Model: Lγ vs. $L_{spin}$

First, **analytically** consider the condition of self-sustained OG. An OG emits the energy flux (KH 2008, ApJ 688, L25)

$$(\nu F_\nu)_{peak} \approx 0.0450 h_m^{\ 3} \frac{\mu^2\Omega^4}{c^3}\frac{1}{d^2},$$

by curvature process, where $h_m$ denotes dimensionless OG trans-***B*** thickness, $\mu$ the dipole moment, and $d$ the distance.

OG luminosity can be, therefore, evaluated as

$$L_\gamma \approx 2.36(\nu F_\nu)_{peak} \times 4\pi d^2 f_\Omega \approx 1.23 f_\Omega h_m^{\ 3} \underbrace{\frac{\mu^2\Omega^4}{c^3}}_{\propto \dot{E}}.$$

Thus, $h_m$ controls the luminosity evolution.

## §7 Modern OG Model: Lγ vs. $L_{spin}$

To examine $h_m$, consider the condition of self-sustained OG.

An inward e⁻ emits $N_\gamma^{in}$~$10^4$ synchro-curvature photons, $N_\gamma^{in}\tau^{in}$~10 of which materialize as pairs.

Each returned, outward e⁺ emits $N_\gamma^{out}$~$10^5$ curvature photons, $N_\gamma^{out}\tau^{out}$~0.1 of which materialize as pairs.

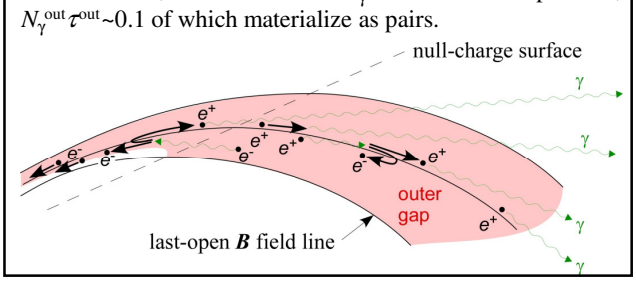


## §7 Modern OG Model: Lγ vs. $L_{spin}$

To examine $h_m$, consider the condition of self-sustained OG.

An inward e⁻ emits $N_\gamma^{in}$~$10^4$ synchro-curvature photons, $N_\gamma^{in}\tau^{in}$~10 of which materialize as pairs.

Each returned, outward e⁺ emits $N_\gamma^{out}$~$10^5$ curvature photons, $N_\gamma^{out}\tau^{out}$~0.1 of which materialize as pairs.

That is, gap trans-***B***-field thickness $h_m$ is automatically regulated so that $N_\gamma^{in}\tau^{in}N_\gamma^{out}\tau^{out}=1$ is satisfied.

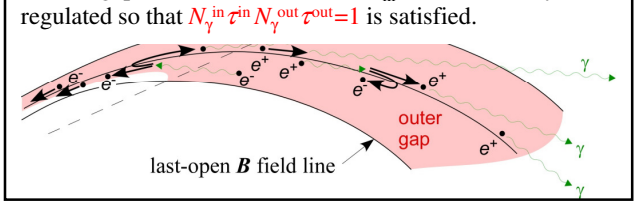

## §7 Modern OG Model: $L_\gamma$ vs. $L_{spin}$

**Step 1:** Both $N_\gamma^{in}\tau^{in}$ and $N_\gamma^{out}\tau^{out}$ are expressed in terms of $P,\mu,\alpha,T$, and $h_m$. Thus, $N_\gamma^{in}\tau^{in}N_\gamma^{out}\tau^{out}=1$ gives $h_m = h_m(P,\mu,\alpha,T)$.

**Step 2:** Specifying the spin-down law, $P=P(t,\alpha)$, and the cooling curve, $T=T(t)$, we can solve $h_m = h_m(t,\alpha)$.

**Step 3:** On the other hand, $P=P(t,\alpha)$ gives $\dot{E} = \dot{E}(t,\alpha)$.

**Step 4:** Therefore, we can relate $L_\gamma \propto h_m^{\,3}\dot{E}$ and $\dot{E}$ with intermediate parameter, pulsar age, $t$.

## §7 Modern OG Model: $L_\gamma$ vs. $L_{spin}$

**Step 1:** express $N_\gamma^{in}\tau^{in}$ and $N_\gamma^{out}\tau^{out}$ with $P,\mu,\alpha,kT$, $h_m$.

OG model predicts

$$E_\parallel \approx \frac{\mu}{2\varpi_{LC}^{\,3}} h_m^{\,2}.$$

Particles ($e^\pm$'s) saturate at Lorentz factor,

$$\gamma = \left(\frac{3\rho_c^2}{2e}E_\parallel\right)^{1/4},$$

emitting curvature photons with characteristic energy,

$$h\nu_c = \frac{3}{2}\hbar c\frac{\gamma^3}{\rho_c}.$$

## §7 Modern OG Model: $L_\gamma$ vs. $L_{spin}$

**Step 1:** express $N_\gamma^{in}\tau^{in}$ and $N_\gamma^{out}\tau^{out}$ with $P,\mu,\alpha,T$, $h_m$.

An inward $e^-$ or an outward $e^+$ emits

$$(N_\gamma)^{in} = eE_\parallel l_2 / h\nu_c, \quad (N_\gamma)^{out} = eE_\parallel l_1 / h\nu_c$$

photons while running the distance $l_2$ or $l_1$.

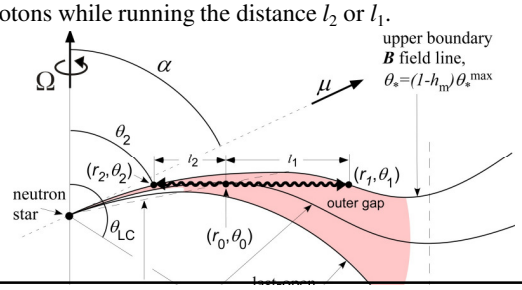


## §7 Modern OG Model: $L_\gamma$ vs. $L_{spin}$

**Step 1:** express $N_\gamma^{in}\tau^{in}$ and $N_\gamma^{out}\tau^{out}$ with $P,\mu,\alpha,T$, $h_m$.

An inward $e^-$ or an outward $e^+$ emits

$$(N_\gamma)^{in} = eE_\parallel l_2 / h\nu_c, \quad (N_\gamma)^{out} = eE_\parallel l_1 / h\nu_c$$

photons while running the distance $l_2$ or $l_1$.

Such photons materialize as pairs with probability

$$\tau^{in} = l_2 F_2 \sigma_2 / c, \quad \tau^{out} = l_1 F_1 \sigma_1 / c$$

where $F_1$, $F_2$ denotes the X-ray flux and $\sigma_1$, $\sigma_2$ the pair-production cross section.

Quantities $l_1$, $l_2$, $F_1$, $F_2$, $\sigma_1$, $\sigma_2$ can be expressed by $P,\mu,\alpha,T$, and $h_m$, if we specify the $\boldsymbol{B}$ field configuration.

## §7 Modern OG Model: Lγ vs. $L_{spin}$

**Step 2:** Give spin-down law and NS cooling curve.

Assume dipole-radiation formula,

$$-I\Omega\dot{\Omega} = \frac{2}{3}\frac{\mu^2\Omega^4}{c^3} \quad \rightarrow \; P = P(t,\alpha)$$

Adopt the minimum cooling scenario (i.e., without any direct-Urca, rapid cooling processes).

$$\rightarrow \; T = T(t)$$

## §7 Modern OG Model: Lγ vs. $L_{spin}$

Cooling curves in the minimum cooling scenario:

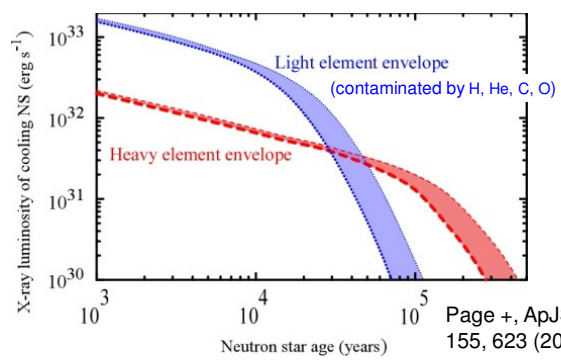


Page +, ApJS 155, 623 (2004)

## §7 Modern OG Model: Lγ vs. $L_{spin}$

**Step 2:** Now we can solve $h_m = h_m(t)$.

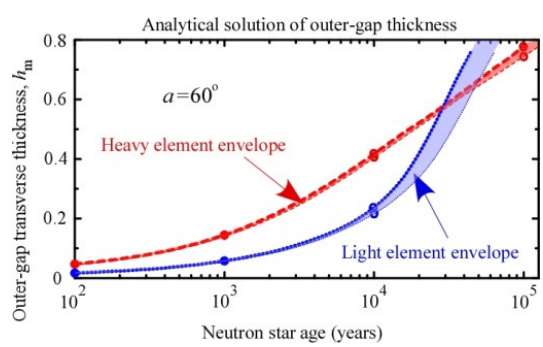


## §7 Modern OG Model: Lγ vs. $L_{spin}$

**Step 3:** We can immediately solve $\dot{E} = \dot{E}(t,\alpha)$ by the spin-down law.

$$\dot{E} = -I\Omega\dot{\Omega} = C\frac{\mu^2\Omega^4}{c^3} \;,$$

for magnetic dipole braking, $C = \frac{2}{3}\sin^2\theta$

Assuming $\alpha$=90°, and noting $\Omega = 2\pi/P$, we obtain

$$P = 39.2\mu_{30}I_{45}^{-1/2}\left(t/10^3\,\mathrm{yr}\right)^{1/2} \;\; \mathrm{ms}$$

and hence $\dot{E} = \dot{E}(t,\alpha)$

## §7 Modern OG Model: Lγ vs. $L_{spin}$

**Step 4:** Use $h_m = h_m(t)$ to relate $L_\gamma \propto h_m^{\,3}\,\dot{E}$ with $\dot{E} = \dot{E}(t)$.

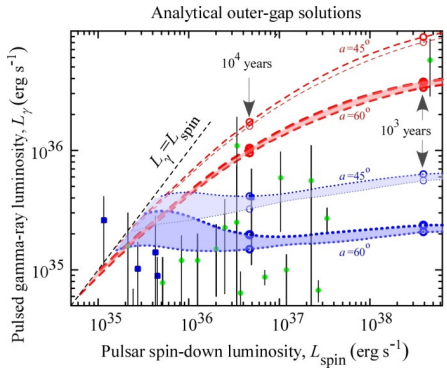


## §7 Modern OG Model: Lγ vs. $L_{spin}$

Second, let us derive the evolution of $L_\gamma$ numerically.

For this purpose, we simultaneously solve

(1) Poisson eq. for electrostatic potential,
(2) Boltzmann eqs. for electrons/positrons,
(3) Radiative transfer eq. for emitted photons

in the 3-D pulsar magnetosphere under the BDCs,

(a) inner BD= NS surface,
(b) lower BD= last-open ***B*** lines,
(c) outer, upper BD is determined as a free-BD,
(d) No $e^\pm$ injection across inner/outer BDs,
(e) No photon injection across inner/outer BDs.

## §7 Modern OG Model: Lγ vs. $L_{spin}$

The Poisson equation for the electrostatic potential ψ is given by

$$-\nabla^2\psi = 4\pi(\rho - \rho_{GJ}) \ ,$$

where

$$E_\parallel \equiv -\frac{\partial\Psi}{\partial x} \ , \ \rho_{GJ} \equiv -\frac{\mathbf{\Omega}\bullet\mathbf{B}}{2\pi c},$$

$$\rho \equiv e\int_0^\infty d\mathbf{p}^3\left[N_+(\mathbf{x},\mathbf{p}) - N_-(\mathbf{x},\mathbf{p})\right] + \rho_{ion} \ .$$

$N_+/N_-$: distrib. func. of $e^+/e^-$
$\boldsymbol{p}$ : momentum of $e^+/e^-$

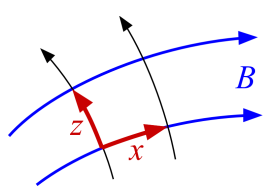


## §7 Modern OG Model: Lγ vs. $L_{spin}$

Assuming $\partial_t + \Omega\partial_\phi = 0$ , we solve the $e^\pm$'s Boltzmann eqs.

$$\frac{\partial N_\pm}{\partial t} + \vec{v}\cdot\nabla N_\pm + \left(e\vec{E}_\parallel + \frac{\vec{v}}{c}\times\vec{B}\right)\cdot\frac{\partial N_\pm}{\partial\vec{p}} = S_{IC} + S_{SC} + \int\alpha_\nu d\nu\int\frac{I_\nu}{h\nu}d\omega$$

together with the radiative transfer equation,

$$\frac{dI_\nu}{dl} = -\alpha_\nu I_\nu + j_\nu$$

$N_\pm$: positronic/electronic spatial # density,
$E_\parallel$: mangnetic-field-aligned electric field,
$S_{IC}$: ICS re-distribution function, $d\omega$: solid angle element,
$I_\nu$: specific intensity, $l$ : path length along the ray
$\alpha_\nu$: absorption coefficient, $j_\nu$: emission coefficient

## §7 Modern OG Model: $L\gamma$ vs. $L_{spin}$

Numerical solution is consistent with the analytical one.

$L\gamma \sim L_{spin}^{0\text{-}0.4}$ if $L_{spin} > 10^{36}$ erg/s

However, $L\gamma$ declines rapidly if $L_{spin} < 10^{35.5}$ erg/s

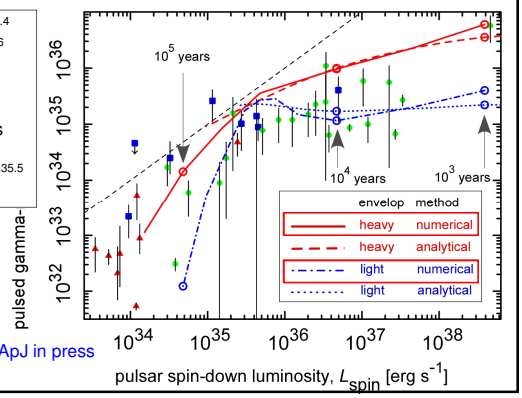


KH (2013) ApJ in press

## §7 Modern OG Model: $L\gamma$ vs. $L_{spin}$

Numerical solution is consistent with the analytical one.

For light element envelop, $L\gamma$ peaks around 30 kyrs, as predicted by analytical calculation.

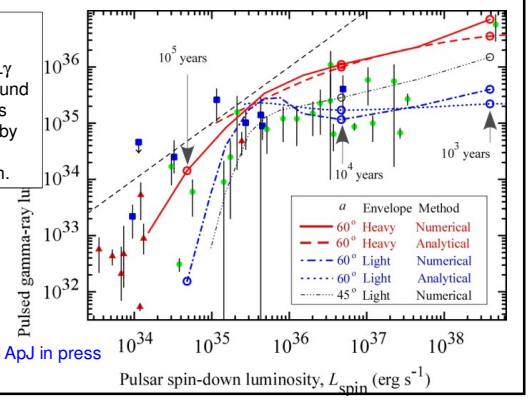


KH (2013) ApJ in press

## §7 Modern OG Model: $L\gamma$ vs. $L_{spin}$

It is worth examining the curvature photon energy, $h\nu_c$.

$h\nu_c$ is regulated below several GeV by self-sustained OG.

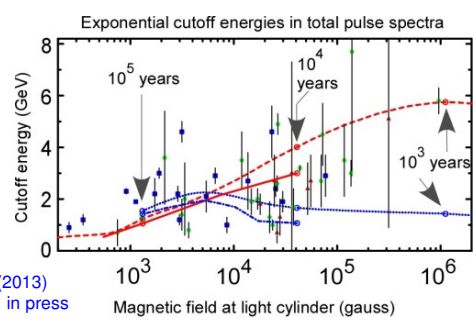


KH (2013) ApJ in press

## §7 Modern OG Model: $L\gamma$ vs. $L_{spin}$

Finally, take a look at the flux correction factor $f_\Omega$, where $L_\gamma = 4\pi f_\Omega F_\gamma d^2$.

Emission is more beamed along equator as pulsar ages.

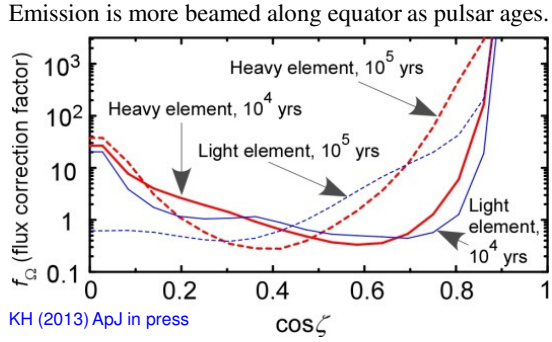


KH (2013) ApJ in press

## *Summary*

- We can now solve pulsed high-energy emissions from the set of Maxwell (div$\boldsymbol{E}$=4π$\rho$) and Boltzmann eqs., if we specify $P$, $dP/dt$, $\alpha_{\rm incl}$, $kT_{\rm NS}$. We no longer have to assume the gap geometry, $E_{\parallel}$, $e^{\pm}$ distribution functions.
- Gamma-ray luminosity evolves as

$$L_{\gamma} \propto \dot{E}^{0-0.4} \quad \text{when} \quad \dot{E} > 10^{36.5}\ \text{erg s}^{-1}$$

However, it declines more rapidly at $\dot{E} < 10^{36.5}$ erg s$^{-1}$ , because created current becomes much less than GJ value.

- Curvature cutoff energy is self-regulated below several GeV, because $h_{\rm m}$ is suppressed by $E_{\parallel}$ screening due to the polarization of produced pairs.